Kinetochore-centrosome feedback linking CENP-E and Aurora kinases controls chromosome congression

Kruno Vukušić*, Iva M. Tolić*

Division of Molecular Biology, Ruđer Bošković Institute, Zagreb, Croatia

*Corresponding authors

E-mail: kvukusic@irb.hr, tolic@irb.hr

ABSTRACT

Chromosome congression is crucial for accurate cell division, with key roles played by kinetochore components such as CENP-E/kinesin-7 and Aurora B kinase. However, Aurora kinases can both inhibit and promote congression, suggesting the presence of a larger, yet poorly understood, signaling network. Our study demonstrates that centrosomes primarily inhibit congression initiation when CENP-E is inactive or absent by regulating the activity of kinetochore components. Depleting centrioles via Plk4 inhibition allows chromosomes near acentriolar poles to initiate congression independently of CENP-E. In contrast, at centriolar poles high Aurora A activity enhances Aurora B activity, increasing phosphorylation of microtubule-binding proteins at kinetochores and preventing stable microtubule attachments in the absence of CENP-E. Conversely, inhibiting Aurora A reduces Aurora B activity, enabling congression initiation even without CENP-E. These findings suggest a feedback network involving Aurora kinases and CENP-E that regulates timing of chromosome movement by modulating kinetochore-microtubule interactions, with centrosomes and the Aurora A activity gradient providing critical spatial cues for the network's function.

Keywords: Mitosis/Centrosome/Chromosome congression/Kinetochore/Aurora kinases/CENP-E

INSTRODUCTION

Chromosome congression, the process by which chromosomes align at the spindle equator during early mitosis, is essential for accurate chromosome segregation and cell division (Ferreira and Maiato, 2021; Kops et al., 2010). The kinetochore motor protein CENP-E (Centromere-associated protein E) is recognized as a critical player in this process (Maiato et al., 2017; Kops et al., 2010; Barisic and Rajendraprasad, 2021; Craske and Welburn, 2020; Auckland and McAinsh, 2015). The prevailing view of CENP-E's role during congression is that its motor activity moves chromosomes along microtubules to the spindle midplane, independently of their biorientation (Kapoor et al., 2006; Barisic et al., 2014, 2015; Kim et al., 2010). However, our recent observations challenge this understanding of CENP-E's function in congression. We propose that chromosome congression is coupled to biorientation near the spindle poles through CENP-E, which stabilizes end-on attachments at polar kinetochores via its interaction with BubR1 (Vukušić & Tolić, 2024). Notably, CENP-E is essential only for the congression of chromosomes near centrosomes (Barisic et al., 2014; Barisic and Maiato, 2015), and biorientation in unperturbed spindles occurs only outside the centrosome-proximal regions (Renda et al., 2022; Renda and Khodjakov, 2021). Yet, the role of centrosome signaling in both chromosome biorientation and congression is unclear.

Centrosomes are non-membranous organelles involved in various cellular processes, including cell division and ciliogenesis (Conduit et al., 2015). Most vertebrate somatic cells contain two centrosomes, each centered around a pair of centrioles. These cylindrical structures, composed of microtubules arranged in a nine-fold symmetry, anchor and organize the pericentriolar material, which is crucial for microtubule nucleation and spindle formation (Conduit et al., 2015). Previous studies have demonstrated that centrioles are not essential for chromosome segregation in mitotic vertebrate cells (Wong et al., 2015; Khodjakov et al., 2000), and in oocytes which naturally lack centrioles (Manandhar et al., 2005). Centrosome-associated kinases such as Aurora A are critical for centrosome maturation, which involves enlargement, increased microtubule nucleation capacity, and the establishment of spindle poles prior to mitosis (Vasquez-Limeta and Loncarek, 2021). Regarding chromosome movement, Aurora kinases are known to activate CENP-E through phosphorylation, thereby promoting chromosome congression in the vicinity of centrosomes (Eibes et al., 2023; Kim et al., 2010). However, we have recently shown that Aurora kinases also inhibit congression initiation when CENP-E is inactive of absent (Vukušić & Tolić, 2024). These seemingly paradoxical activities of Aurora kinases within the same process suggest the existence of signaling feedback among different components of the mitotic spindle. However, the nature of this feedback and its regulation remain unknown.

In this study, we investigate the role of centrosomes in regulating chromosome congression under varying levels of CENP-E activity by combining RNAi, acute chemical inhibition, and large-scale live-cell imaging approaches. Our findings reveal that centrioles, through the activity of Aurora A kinase, inhibit the congression of polar chromosomes when CENP-E is non-functional. By depleting centrioles through Polo-like kinase 4 (Plk4) inhibition, we show that acentriolar poles enable chromosomes to initiate congression independently of CENP-E, in contrast to centriolar poles. This inhibitory effect of centrioles is mediated by high Aurora A activity at centriolar poles. We found that Aurora A activates Aurora B at kinetochores near centrosomes, which increases the phosphorylation of KMN network (the Knl1 complex, the Mis12 complex and the Ndc80 complex) and prevents stable microtubule attachments on kinetochores. We thus propose a negative

feedback loop in which Aurora B kinase, activated by Aurora A near centrosomes, destabilizes end-on attachments at the spindle poles, while CENP-E, also activated by Aurora kinases, counteracts this destabilization to promote chromosome congression. These insights offer a new understanding of the complex molecular interplay between centrosomes and kinetochores during chromosome congression.

RESULTS

Centrioles prevent the initiation of chromosome congression when CENP-E is absent.

Polar chromosomes, in the absence of CENP-E, remain localized near the centrosomes for extended periods before initiating chromosome congression (Barisic et al., 2014; Tovini and McClelland, 2019). Based on this, we hypothesized that centrosomes might inhibit the initiation of congression of polar chromosomes when CENP-E is inactive or absent. To test this hypothesis, we imaged non-transformed human cells expressing CENP-A-GFP and centrin1-GFP (Magidson et al., 2011) by confocal microscopy after acute reactivation of CENP-E and after depletion of CENP-E by RNA interference (Fig. S1A and B) (Vukušić & Tolić, 2024). We then tracked the movement of polar kinetochores over time (see Methods) and measured the duration of congression as a proxy of the likelihood of congression initiation for each pair of sister kinetochores with respect to their distance from the nearest centrosome. From this analysis, we found that the likelihood of congression initiation increases with the distance of the kinetochore pair from the centrosome, prominently in the absence of CENP-E and weakly after its acute reactivation (Fig. S1C and D). This suggests that centrosomes play an inhibitory role in the initiation of congression in the absence of CENP-E.

To investigate the role of centrosomes in chromosome congression in more detail, we employed a targeted imaging assay designed to systematically explore the interplay between key molecular structures at kinetochores and centrosomes during this process. Using the advanced lattice light-sheet microscopy approach described in the accompanying manuscript (Vukušić & Tolić, 2024), we captured high-resolution time-lapse images of live mitotic cells with labelled centromeres and centrosomes. We combined this imaging approach with CENP-E perturbation techniques that allowed us to vary CENP-E activity: CENP-E depletion, CENP-E inhibition, and control DMSO-treated cells (Vukušić & Tolić, 2024) (Fig. 1A). If centrosomes inhibit the congression of polar chromosomes in the absence of CENP-E, as we hypothesized, we reasoned that depleting centrioles, might allow polar chromosomes to undergo congression independently of CENP-E. To deplete centrioles, we inhibited polo-like kinase 4 (Plk4) activity using centrinone, a small molecule inhibitor that blocks the centriole duplication cycle (Wong et al., 2015). By varying the duration of treatment, we generated spindles with different numbers of centrioles at each pole—specifically 2:2 without treatment, 1:1 after one day, 1:0 after two days, and 0:0 after more than three days of treatment—and combined these with CENP-E perturbations (Fig. 1A and B).

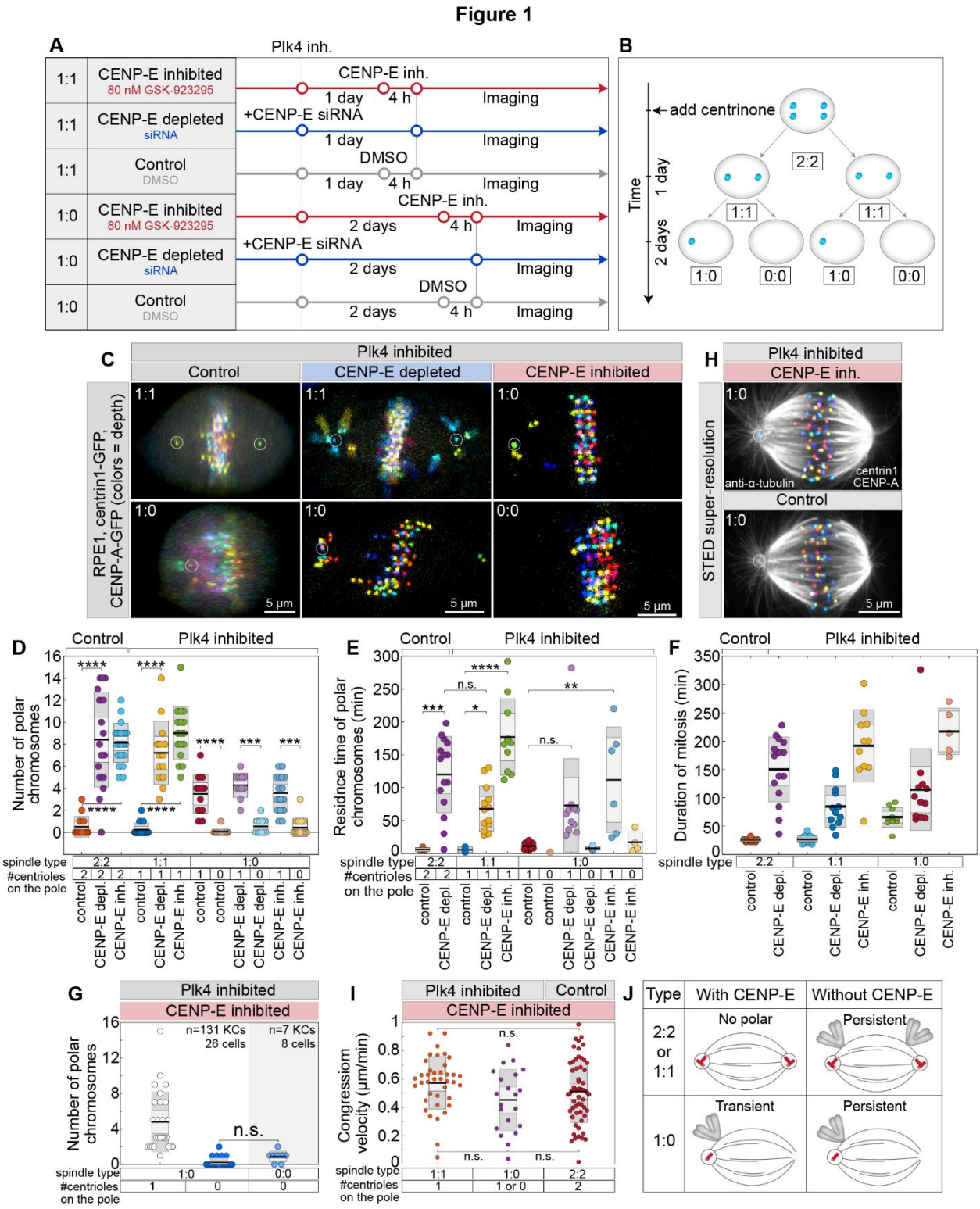

Figure 1. Centrioles inhibit chromosome congression initiation in the absence of CENP-E activity. (A) Scheme of the protocol to obtain varying and acutely controllable levels of CENP-E activity in cells in combination with different numbers of centrioles on each spindle pole. (B) Scheme depicting progressive centriole depletion in mitotic cells following continuous Plk4

inhibition by 300 nM centrinone. (C) Representative examples of live-imaged cells expressing CENP-A-GFP and centrin1-GFP with different numbers of centrioles on each pole, denoted by white circles, 5 minutes after spindle elongation, for treatments indicated on top. (D-F) Number (D), residence time on spindle pole (E) of polar chromosomes after the end of prometaphase spindle elongation, and duration of mitosis (F) in cells with different numbers of centrioles as indicated and across different treatments depicted on bottom. The category “1” contains data from centriolar spindle poles from both 1:1 and 1:0 spindles. The black line shows the mean; the light grey and dark grey areas mark the 95% confidence interval on the mean and standard deviation, respectively. Number of cells per condition (D-F): 14, 15, 22, 16, 14, 18, 16, 16, 12, 12, 16, 16, each from at least three independent biological replicates. (G) Number of polar chromosomes after different treatments of cells with different numbers of centrioles as indicated. Cells were fixed prior to measurement. Experiment performed in more than three independent biological replicates. (H) Representative examples of RPE-1 cells after treatments indicated at the top immunostained for α-tubulin and imaged by stimulated emission depletion (STED) microscopy in cells expressing CENP-A-GFP and centrin1-GFP. Projection is color-coded by depth as specified by the color bar in Figure 1A. (I) Velocity of chromosome movement during the 6-minute period that precedes complete alignment for each initially polar kinetochore pair in different treatments and number of centrioles. (J) Schemes depicting the summary of experimental results for the number and residence time of polar chromosomes on spindle poles for cells characterized by different numbers of centrioles with or without CENP-E activity. All images are maximum projections color-coded by height as specified on the color bar in 1A. Statistics: Tukey's HSD test. Symbols indicate: n.s. $P > 0.05$, *$P \leq 0.05$, **$P \leq 0.01$, ***$P \leq 0.001$, ****$P \leq 0.0001$. inh., inhibited; depl., depleted; siRNA, small interfering RNA.

As a proxy for congression efficiency, we quantified the number of polar chromosomes 5 minutes after spindle elongation, the residence time of polar chromosomes at the spindle poles, and the total duration of mitosis (see Methods). Following CENP-E perturbations, spindles with a 1:1 or 2:2 centriole configuration had an average of about eight polar chromosomes per spindle, compared to fewer than one chromosome under control conditions in both spindle types (Fig. 1C and D; and Video 1). In 1:0 spindles, the centriolar poles (labeled "1") contained approximately four polar chromosomes, similar to their counterparts in 1:1 spindles (Fig. 2B; and Video 1). The occurrence of polar chromosomes at centriolar poles in 1:0 spindles was independent of CENP-E activity (Fig. 2D). The acentriolar poles (labeled "0") in 1:0 spindles consistently had an average of around one polar chromosome, regardless of CENP-E activity (Fig. 1C and D; and Video 1). Importantly, polar chromosomes persisted significantly longer at centriolar poles than at acentriolar poles across all spindle types when CENP-E was perturbed (Fig. 1E), resulting in a marked prolongation of mitosis (Fig. 1F). Furthermore, completely acentriolar 0:0 spindles, which were rarely observed due to p53-dependent arrest (Wong et al., 2015), exhibited a low number of polar chromosomes under CENP-E inhibition, similar to the acentriolar poles in 1:0 spindles (Fig. 1C and G; and Video 1). These findings suggest that centrioles specifically limit the initiation of polar chromosome congression when CENP-E activity is compromised.

The low number of polar chromosomes at acentriolar poles could be a result of the transient monopolarization of 1:0 spindles (Dudka et al., 2019). However, we observed that forced transient monopolarization through Eg5 inhibitor washout, followed by CENP-E inhibition, did not increase the number of polar chromosomes compared to untreated spindles (Fig. S2A) (Vukušić & Tolić, 2024). This suggests that the inhibitory effect of centrioles on polar chromosome congression in 1:0 spindles without CENP-E is independent of passage through the transient monopolar state. To observe differences in microtubule organization between centriolar and acentriolar poles we imaged microtubules using STED microscopy. However, we observed no significant differences in microtubule organization between centriolar and acentriolar poles, aside from the absence of astral microtubules at the acentriolar pole (Fig. 1H).

To determine whether the inhibitory effect of centrioles on congression is dependent on chronic Plk4 inhibition, we investigated whether centriole dislocation from spindle pole during prolonged mitosis could induce the congression of polar chromosomes independently of the long-term effects of Plk4 inhibition. We focused on rare instances (<10%, n=5 out of 55 cells) where spontaneous acute dislocation of a centriole from the spindle pole occurred in 1:1 spindles under CENP-E depletion (Fig. S2B) (McEwen et al., 2001). Fascinatingly, in all observed cases, polar chromosomes initiated congression almost immediately following the displacement of a centriole from the centrosome (Fig. S2B). This finding suggests that the mere presence of centrioles limits the congression of polar chromosomes in the absence of CENP-E.

How is congression movement influenced by the absence or reduced number of centrioles? Congression velocities were indistinguishable between 1:1 and 1:0 spindles, as well as from those observed in 2:2 spindles following CENP-E inhibition (Fig. 1I, and S2C-G) (Vukušić & Tolić, 2024). This result suggest that centrioles affect congression initiation but not the movement of polar chromosomes to the metaphase plate. In conclusion, the presence of centrioles is essential for the persistence of polar chromosomes when CENP-E activity is absent (Fig. 1J), demonstrating that centrioles actively inhibit the initiation of congression of polar chromosomes.

Centriolar Aurora A increases kinetochore Aurora B activity, leading to increased KMN network phosphorylation and delayed congression initiation in the absence of CENP-E

What molecular factors are responsible for inhibiting congression initiation near centrioles in the absence of CENP-E? Since inhibition of Aurora A kinase induces the congression of polar chromosomes in the absence of CENP-E or its activity (Vukušić & Tolić, 2024), we hypothesized that Aurora A activity inhibits chromosome congression at centriolar poles when CENP-E is absent. To test this hypothesis, we quantified the levels of active Aurora A (pAurA, pT288-Aurora A) on spindle poles with varying numbers of centrioles after Plk4 inhibition, under both control and CENP-E inhibited conditions. Intriguingly, we found that acentriolar poles exhibited a 4-fold lower level of pAurA compared to centriolar poles, whereas the maximum difference between the two poles in 1:1 spindles was, on average, only 10% (Fig. 2A and B). The observed difference in pAurA levels between poles was not dependent on CENP-E (Fig. 2A and B), suggesting that CENP-E does not regulate the level of active Aurora A at spindle poles. These findings, combined with our observation that Aurora A inhibition promotes congression in the absence of CENP-E

(Vukušić & Tolić, 2024), indicate that polar chromosomes rely on CENP-E activity for congression due to the high activity of Aurora A near centrosomes.

Figure 2

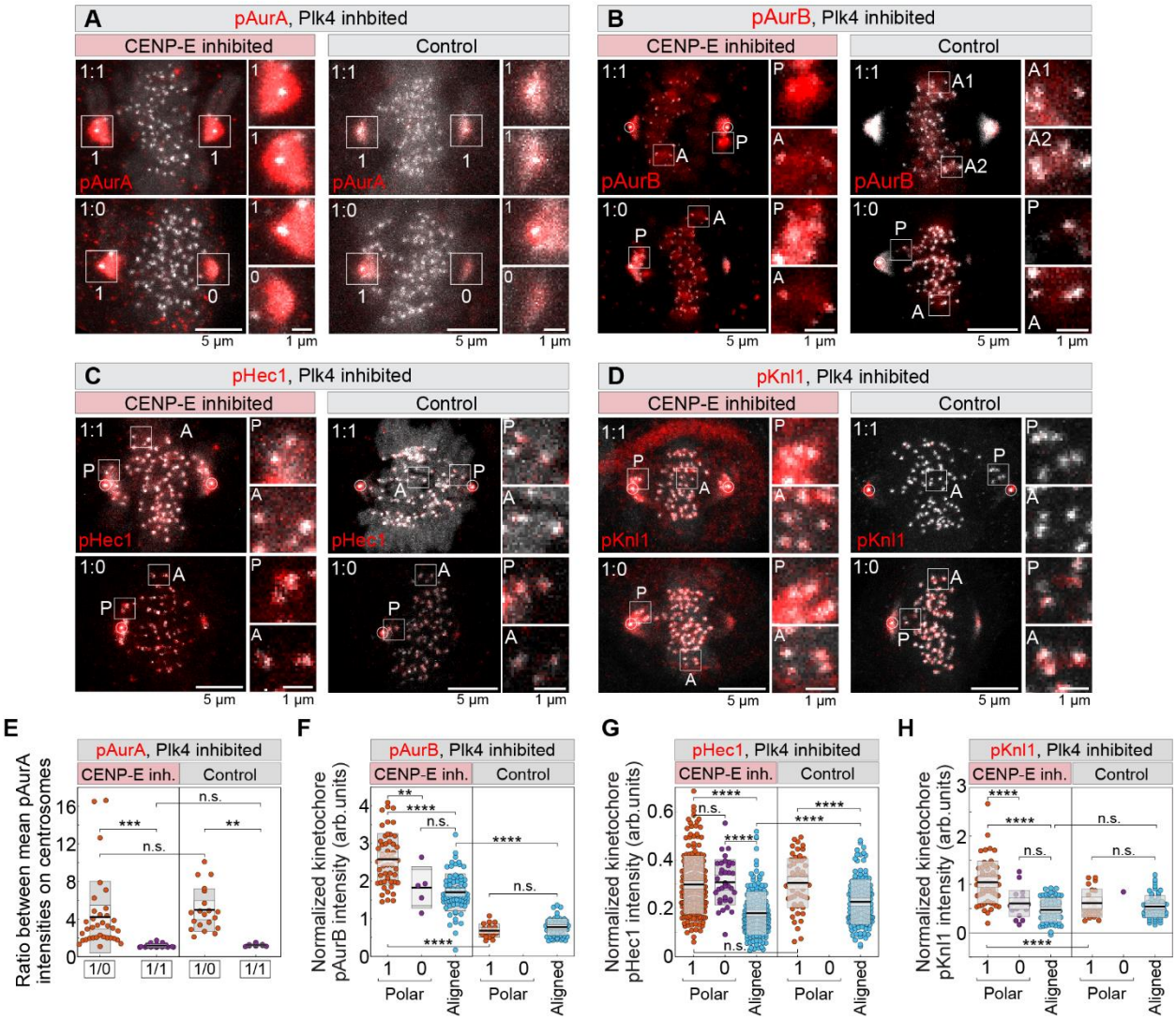

Figure 2. Centriolar Aurora A activity is linked to increased activity of kinetochore Aurora B and its downstream KMN network targets in the absence of CENP-E activity. (A-D) Representative examples of cells expressing CENP-A-GFP and centrin1-GFP (grey), with centrioles denoted by white circles, immunostained with antibodies targeting phosphorylated (p) residues of indicated proteins (red) (pT288-Aurora A, pT232-Aurora B, pS55-Hec1, and pS24, pS60-Knl1) with different numbers of centrioles on each pole as depicted, after treatments as indicated on top, and with enlarged insets of boxed areas on the right. The images are maximum projections. P, polar. A, aligned. (E-H) Ratio between the mean phosphorylated Aurora A in the centriolar spindle pole ("1") versus the acentriolar pole ("0") for the indicated treatments (E), the mean intensity of the targeted phosphorylated residues in the kinetochore as indicated and normalized to the kinetochore CENP-A intensity for the indicated kinetochore proteins, different treatments and centriolar numbers (F-H). Numbers: 88 cells (E), 179 kinetochores from 42 cells

(F), 594 kinetochores from 67 cells (G), 227 kinetochores from 63 cells (H), all done in at least two independent biological replicates. Statistics: Tukey's HSD test. Symbols indicate: n.s. $P > 0.05$, $^{**}P \leq 0.01$, $^{***}P \leq 0.001$, $^{****}P \leq 0.0001$. Inh., inhibited; depl., depleted; chr., chromosomes; NT, non-targeting; KC, kinetochore; arb., arbitrary.

We hypothesized that the high Aurora A activity at centriolar spindle poles might lead to increased activation of kinetochore-localized Aurora B kinase on polar chromosomes. High Aurora B activity would affect the phosphorylation of its downstream targets, Hec1 and Knl1, which are key components of the KMN network (Navarro and Cheeseman, 2021), thus blocking congression. Indeed, we observed that the mean signals of pAurB (pT232-Aurora B) and pKnl1 (pS24, pS60-Knl1) (Welburn et al., 2010) on polar kinetochores near centriolar poles were significantly higher compared to aligned kinetochores and the rare polar kinetochores at acentriolar poles when CENP-E was inhibited (Fig. 2C-H; and Fig. S3A and B). Curiously, for pHec1 at the phosphorylation site dependent on both Aurora A and B activities (pS55-Hec1) (DeLuca et al., 2006, 2018), a significant difference was observed only between polar and aligned kinetochores (Ye et al., 2015; DeLuca et al., 2018) (Fig. 2E and F). In control cells, the phosphorylation levels of pAurB, pKnl1, and pHec1 were similar between aligned and rare polar kinetochores and were significantly lower compared to these kinetochore groups under CENP-E inhibition for pAurB and pKnl1 (Fig. 2C-H). These results suggest that in the absence of CENP-E activity, Aurora A at centriolar poles enhances the activity of outer kinetochore Aurora B. This elevated Aurora B activity increases the phosphorylation of downstream outer kinetochore proteins, such as Knl1 and, to a lesser extent, Hec1 at the S55 site. This phosphorylation inhibits the stabilization of end-on microtubule attachment to kinetochores, thereby preventing chromosome congression.

Aurora A directly enhances activity of Aurora B close to centrosomes

Based on our results, we hypothesized that Aurora A at centrosomes directly regulates the activity of Aurora B at kinetochores. To determine whether Aurora A directly regulates Aurora B activity on polar kinetochores in the absence of CENP-E, we inhibited Aurora A by MLN8237 (Görgün et al., 2010) in CENP-E-depleted cells using different concentrations and durations of inhibition. We then performed immunofluorescence staining for pAurB and quantified its levels on kinetochores at different time points (Fig. 3A). Our results showed that inhibiting Aurora A significantly reduced Aurora B activity on polar kinetochores, bringing it down to levels comparable to those observed on aligned kinetochores in the absence of CENP-E (Fig. 3A-C). These findings support a model in which Aurora A at spindle poles enhances Aurora B activity when CENP-E is inactive (Fig. 3D). This elevated Aurora B activity inhibits end-on microtubule attachments and contributes to mitotic delays.

Figure 3

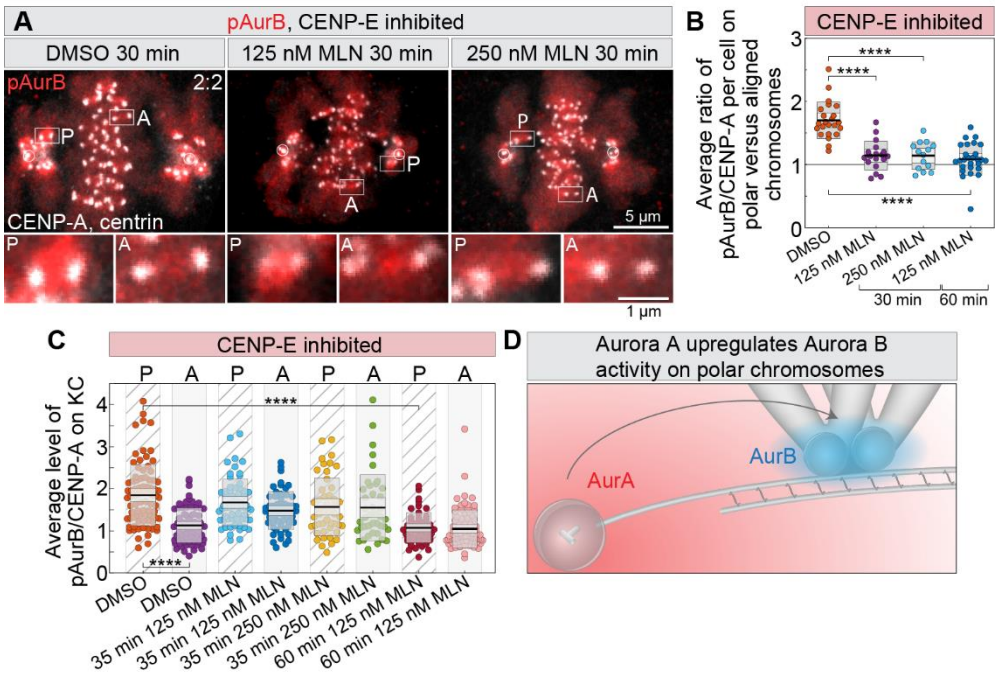

Figure 3. Aurora A directly upregulates Aurora B activity. (A) Representative examples of cells expressing CENP-A-GFP and centrin1-GFP (grey), with centrioles denoted by white circles, after treatments as indicated on top, and with enlarged insets of boxed areas. Cells were immunostained with antibodies targeting pT232-Aurora B (red). (B) The average ratio of mean intensities of pT232-Aurora B normalized to CENP-A on polar versus on aligned kinetochores per each cell in the indicated treatments. MLN, MLN8237. (C) The average level of pT232-Aurora B normalized to the average level of CENP-A on kinetochores (KC) after treatments indicated at the bottom. P, polar; A, aligned. (D) Scheme depicting the model based on experimental results in which the Aurora A activity gradient on centriolar centrosomes (red gradient centered on centrioles) upregulates Aurora B activity on polar kinetochores (blue gradient on kinetochores) that limits the establishment of end-on attachments in the absence of CENP-E, while a low level of active Aurora B on kinetochores leads to the establishment of end-on attachments and chromosome congression independently of CENP-E. Numbers: 571 kinetochore pairs from 91 cells (B and C), all done in at least two independent biological replicates. n.s., nonsignificant. Statistics: Tukey's HSD test. Symbols indicate: n.s. $P > 0.05$, $^{**}P \leq 0.01$, $^{***}P \leq 0.001$, $^{****}P \leq 0.0001$. KC, kinetochore.

If Aurora A at the centrosomes enhances Aurora B activity, we would expect a decrease in Aurora B-mediated phosphorylation of outer kinetochore targets as chromosomes move away from the centrosome during congression. Indeed, we observed that the level of Aurora B-mediated phosphorylation of Knl1 was inversely correlated with the distance of the chromosome from the centrosome in the absence of CENP-E activity (Fig. S3C). In conclusion, chromosome congression is accompanied by a reduction in Aurora B activity on kinetochores, leading to decreased

phosphorylation of KMN network components. This reduction is crucial for the stable attachment of microtubules to kinetochores (Cheeseman et al., 2006) and is significantly accelerated by the motor activity of CENP-E.

Aurora kinases inhibit congression through regulation of Hec1 phosphorylation

To investigate whether Aurora kinases directly inhibit congression through the regulation of Hec1 phosphorylation, we used HeLa cells engineered to express an inducible, siRNA-resistant GFP-Hec1-9A mutant (Etemad et al., 2015). This mutant mimics the constitutive dephosphorylation of Hec1 at nine phosphorylation sites (DeLuca et al., 2011). Expression of Hec1-9A in the presence of endogenous Hec1 did not affect chromosome alignment (Fig. 4A and C), consistent with previous reports (Etemad et al., 2015; DeLuca et al., 2011). Depletion of Hec1 (Fig. 4B) and CENP-E, as well as inhibition of CENP-E without Hec1-9A overexpression, induced large chromosome misalignments, as expected from previous work (Fig. 4C) (Cai et al., 2009; Barisic et al., 2014). Both depletion and inhibition of CENP-E caused chromosome misalignments in cells expressing endogenous Hec1, even when Hec1-9A was overexpressed (Fig. 4C). This suggests that disruption of CENP-E function cannot be overcome by Hec1-9A overexpression in the presence of endogenous Hec1.

Figure 4

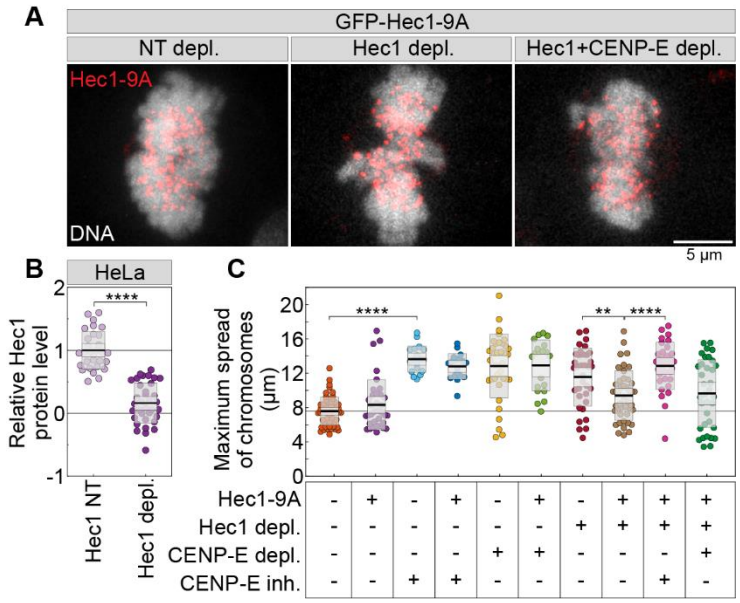

Figure 4. Phosphorylation of Hec1 by Aurora kinases hinders chromosome congression without CENP-E. (A) Representative examples of HeLa cells expressing GFP-Hec1-9A (red) with DNA stained by DAPI (grey) in treatments indicated on the top. (B) Level of Hec1 measured in DNA area stained by DAPI in HeLa cells normalized to the average level of Hec1 in the non-targeting group (NT) after treatments indicated at the bottom. (C) Maximum spread of chromosomes in the indicated treatments, as per the legend on the bottom. Numbers: 571 kinetochore pairs from 91 cells (F), 327 cells (H), all done in at least two independent biological

replicates. Statistics: Tukey's HSD test. Symbols indicate: n.s. $P > 0.05$, **$P \leq 0.01$, ***$P \leq 0.001$, ****$P \leq 0.0001$. Inh., inhibited, depl., depleted; NT, non-targeting; KC, kinetochore.

On the other hand, expression of Hec1-9A in cells with endogenous Hec1 depletion rescued large chromosome misalignments (Fig. 4A and C), as previously reported (DeLuca et al., 2011; Etemad et al., 2015). Based on our finding that acute inhibition of Aurora kinases induces chromosome congression independently of CENP-E (Vukušić & Tolić, 2024), we hypothesized that constitutive dephosphorylation of Hec1 might compensate for disruptions in CENP-E function. Indeed, we found that expressing the non-phosphorylatable Hec1-9A mutant in cells depleted of endogenous Hec1 improved chromosome alignment following CENP-E depletion to levels comparable to when CENP-E was present (Fig. 4A and C). This effect, however, did not occur after CENP-E inhibition (Fig. 4C). These results suggest that Aurora kinase-mediated phosphorylation of Hec1 specifically impedes congression in the absence of CENP-E, consistent with our recent observations using acute kinase inhibition (Vukušić & Tolić, 2024).

DISCUSSION

In this study, we propose that the timing of chromosome movement is regulated by the activity of the CENP-E molecular motor at kinetochores and the chromosomes' proximity to centrosomes, which determines their exposure to the Aurora A gradient (Fig. 5). Previous research has shown that Aurora kinases phosphorylate and activate CENP-E near centrioles (Kim et al., 2010; Eibes et al., 2023). Our recent findings (Vukušić & Tolić, 2024) and the results presented here demonstrate how Aurora kinases inhibit congression initiation in the absence of CENP-E. To reconcile these seemingly conflicting roles of Aurora kinases, we propose a feedback loop where kinetochore activity is influenced by the proximity to centrosomes, where the Aurora A gradient is concentrated (Fig. 5) (Willems et al., 2018). Without CENP-E, Aurora A overactivates Aurora B and its targets, such as KMN complex (DeLuca et al., 2011; Shrestha et al., 2017; Cheeseman et al., 2006; Welburn et al., 2010) and the fibrous corona components (Famulski and Chan, 2007; Cheerambathur et al., 2013), inhibiting end-on attachment stabilization and congression (Vukušić & Tolić, 2024; Ye et al., 2015; Barišić et al., 2014) (Fig. 5). Aurora A also directly phosphorylates KMN components, including Hec1, near centrioles (Ye et al., 2015; DeLuca et al., 2018). though the specific contributions of each Aurora kinase to Hec1 phosphorylation sites (S44, S55, S69 and others) and their roles in congression inhibition remain unclear (DeLuca et al., 2018). Future studies will hopefully clarify this.

When CENP-E is present, it reduces Aurora B activity, promoting end-on attachments and effective congression initiation (Fig. 5) (Vukušić & Tolić, 2024). If the Aurora A gradient is weakened, as in acentriolar centrosomes or after acute Aurora A inhibition, Aurora B activation decreases, allowing end-on attachment and CENP-E-independent congression on polar chromosomes (Fig. 5). However, the weak activity of Aurora kinase is associated with more frequent formation of aberrant attachments of kinetochores to microtubules close to centrosomes, increasing chromosome mis-segregation rates during anaphase in acentriolar or Aurora B inhibited cells (Wong et al., 2015; Ye et al., 2015; Orr et al., 2021). However, during unperturbed mitosis in healthy cells, chromosomes generally avoid regions close to centrosomes and achieve biorientation outside of them (Magidson et al., 2011; Renda et al., 2022; Sikirzhytski et al., 2018), which may explain their rapid congression. The model we presented clarifies the signaling between centrosomes and kinetochores during congression initiation. It explains why pole-proximal kinetochores, which are within the Aurora A gradient, depend on CENP-E for efficient congression in early mitosis (Barisic et al., 2014). This reliance aligns with findings that dephosphorylated Hec1 or acute Aurora kinase inhibition does not interfere with congression (Vukušić & Tolić, 2024), as the KMN network retains maximum microtubule affinity (DeLuca et al., 2011; Etemad et al., 2015), promoting CENP-E-independent congression. Recent findings also show that kinetochores can modulate Aurora A activity via Mps1 (Leça et al., 2024), underscoring the feedback between centrosomes and kinetochores.

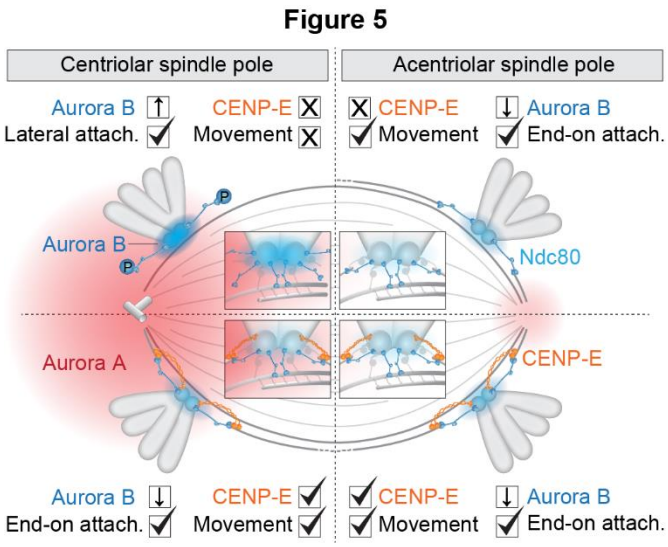

Figure 5. Model of chromosome congression initiation regulation featuring a feedback loop between Aurora B kinase and CENP-E, controlled by the proximity to centrosomal Aurora A kinase. The formation of end-on attachments and the initiation of chromosome congression are controlled by the distance between chromosomes and the centrosome. Polar chromosomes near centriolar centrosomes and without CENP-E (top left quadrant) display lateral kinetochore-microtubule attachments, which fail to quickly convert to stable end-on attachments due to high Aurora A activity (AurA, depicted as a red gradient centered on centrioles, shown as gray tubules). This high Aurora A activity likely activates outer kinetochore-localized Aurora B (AurB, blue gradient centered on the centromere) through phosphorylation. Activated Aurora B phosphorylates (circled P) outer kinetochore proteins, such as Knl1 (not shown) and Hec1 (Ndc80, dark blue), which are essential for stable end-on microtubule attachments and start of chromosome congression. Enlargements of the kinetochore area for each quadrant are shown in the boxed area at the bottom of each quadrant. In the presence of CENP-E, polar chromosomes near centriolar centrosomes (bottom left quadrant) exhibit lower Aurora B activity on kinetochores, which allows the formation of end-on attachments and chromosome biorientation, facilitated by the activities of CENP-E (orange) and BuBR1 (not shown), leading to initiation of chromosome congression toward the spindle midplane. In the absence of centrosomes and CENP-E (top right quadrant), chromosomes near coalesced spindle poles are able to initiate end-on conversion and biorientation independently of CENP-E, due to the absence of a strong Aurora A gradient, resulting in lower Aurora B activity on kinetochores and reduced Hec1 phosphorylation. In this scenario, polar chromosomes move to the spindle equator with dynamics similar to those near centriolar spindle poles. Finally, polar chromosomes located near acentriolar spindle poles in the presence of CENP-E (bottom right quadrant) initiate congression through mechanisms similar to those described for chromosomes near centriolar centrosomes in the presence of CENP-E. Symbols: X represents absence or slow activity, ↓ represents downregulation, ✓ represents presence. Attach., attachment.

Interestingly, overexpression of Aurora A kinase and loss of the CHK2-BRCA1 tumor suppressor pathway—both of which lead to elevated Aurora A activity at centrosomes—are

frequently observed in human cancers (Bischoff et al., 1998; Stolz et al., 2010). Increased Aurora A activity enhances microtubule assembly rates at kinetochores through mechanisms that are not yet fully understood, contributing to chromosomal instability in colorectal cancer cells (Ertych et al., 2014). Our findings suggest that elevated Aurora A activity could impede chromosome congression if not balanced by changes in other key components of the centrosome-kinetochore feedback loop, such as CENP-E/BubR1 and Aurora B kinase. Disruptions in this balance may explain the aberrant congression observed in colorectal cancer cells with overactive Aurora A kinase, which correlates with increased mitotic timing, and chromosome mis-segregation rates in those cells (Ertych et al., 2014).

Aurora A's role as a major inhibitor of chromosome congression might also explain why chromosomes near the poles experience delayed congression, not only in the absence of CENP-E but also in other contexts where CENP-E is active. For example, in multipolar spindles, chromosomes near coalesced spindle poles are often delayed in congression (Ganem et al., 2009), potentially due to their proximity to two centrosomes and their Aurora A gradients. Likewise, cancer cells from various origins frequently struggle with congressing pole-proximal chromosomes, leading to prolonged mitosis (Klaasen et al., 2022; Tamura et al., 2020; Bolhaqueiro et al., 2019). Although the cause of congression problems in cancer cells remains unclear, pole-proximal chromosomes are often mis-segregated into micronuclei, resulting in aneuploidy in both cancer cell line models and patient-derived organoids (Klaasen et al., 2022). We propose that the chromosome congression defects observed in many human tumors may result from imbalances in the signaling feedback described here, leading to disrupted stability of end-on attachments (Bakhoum et al., 2009; Iemura et al., 2021).

Limitations of study

It remains unclear why CENP-E inhibition was not effectively rescued by overexpressing Hec1-9D in the context of Hec1 depletion, unlike with CENP-E depletion. One possibility is that the Hec1-S69 phosphorylation site, absent in the Hec1-9A mutant (DeLuca et al., 2011), is essential for bypassing the need for CENP-E under these conditions. Additionally, the extensive fibrous corona expansion might limit Hec1's engagement with microtubules in the cells with inhibited CENP-E (Cheerambathur et al., 2013). Further research is needed to clarify this. Moreover, Aurora A might have a more direct impact on KMN network components, potentially through specific phosphorylation sites on Hec1, such as S69, which were not examined in this study (DeLuca et al., 2018; Ye et al., 2015). Finally, phospho-specific antibodies can bind non-specifically, especially at centrosomes, potentially affecting results (Welburn et al., 2010). Although care was taken to measure the signals of phospho-antibodies specifically on kinetochores, the potential influence of non-specific binding cannot be completely ruled out.

ACKNOWLEDGEMENTS

We thank Alexey Khodjakov and Geert Kops for cell lines; Marin Barišić, Carlos Conde, Helder Maiato, and Andrea Musacchio for for reviewing and discussing the results; Julie Welburn for discussions and antibodies; Ivana Šarić for the drawings; and members of the Tolić group and Nenad Pavin group for constructive comments on the manuscript. This work was funded by the European Research Council (ERC Synergy Grant, GA Number 855158), the Croatian Science Foundation (HRZZ) through Swiss-Croatian Bilateral Projects (project IPCH-2022-10-9344), and projects co-financed by the Croatian Government and the European Union through the European Regional Development Fund—the Competitiveness and Cohesion Operational Programme: IPSted (Grant KK.01.1.1.04.0057) and QuantiXLie Center of Excellence (Grant KK.01.1.1.01.0004).

AUTHOR CONTRIBUTIONS

K.V. and I.M.T conceived the project, K.V. performed all experiments, quantified, analyzed and presented the data, K.V. conceptualized and prepared original draft, K.V. and I.M.T. reviewed, edited and discussed the manuscript.

MATERIALS & METHODS

Reagents and Tools table

Reagent/Resource	Reference or Source	Identifier or Catalog Number
Experimental Models		
hTERT-RPE1 cells stably expressing CENP-A-GFP, human hTERT-RPE1	Alexey Khodjakov Lab, Wadsworth Center	N/A
hTERT-RPE1 cells stably expressing both CENP-A-GFP and centrin1-GFP	Alexey Khodjakov Lab, Wadsworth Center	N/A
HeLa FlpIn cells expressing GFP-Hec1-9A	Geert Kops Lab, Hubrecht Institute	N/A
Antibodies		
Rabbit monoclonal Anti-NDC80	Sigma-Aldrich	HPA066330
Rat anti-alpha-tubulin YL1/2	Invitrogen	MA1-80017
Donkey anti-rabbit IgG Alexa Fluor 647	Abcam	ab150075
Donkey anti-rabbit IgG Alexa Fluor 594	Abcam	ab150064
Donkey anti-mouse IgG Alexa Fluor 594	Abcam	ab150108
Donkey anti-mouse IgG Alexa Fluor 647	Abcam	ab150107
Donkey anti-rat IgG Alexa Fluor 594	Abcam	ab150156
Oligonucleotides and other sequence-based reagents		
human CENP-E ON-TARGETplus SMART pool siRNA	Dharmacon	L-003252-00-0010
human custom-made 3'UTR HEC1 siRNA, oligo #3	Thermo Fisher Scientific	sequence 5′-CCCUGGGUCGUGUCAGGAA-3′
control siRNA	Dharmacon	D-001810-10-05

Chemicals, Enzymes and other reagents		
MG-132	Merck	M7449
Lipofectamine RNAiMAX Reagent	Thermo	13778150
OPTI-MEM medium	Thermo	31985062
DMEM medium	Thermo	11995065
GSK-923295	MedChemExpress	HY-10299
Monastrol	MedChemExpress	HY-101071A
Centrinone	MedChemExpress	HY-18682
Fetal bovine serum (FBS)	Thermo-Fisher	10270106
µ-Dish 35 mm, high Glass Bottom	Ibidi	81158
35 mm Dish 1.5 Coverslip 10 mm Glass Diameter Uncoated	Mattek	P35G-1.5-10-C
Software		
ImageJ (Fiji)	https://imagej.net/software/fiji/	N/A
Prairie View Imaging Software	Bruker	N/A
Imspector software	Abberior	N/A
ZEN 2.6 software	Zeiss	N/A
MatlabR2021a	MathWorks	
Matlab extension UnivarScatter	https://github.com/manulera/UnivarScatter	N/A
Matlab Statistics Toolbox R14	MathWorks	N/A
Adobe Illustrator CS6	Adobe Systems	N/A
Low Light Tracking Tool (v.0.10) ImageJ plugin	https://imagej.net/plugins/low-light-tracking-tool	N/A
Other		
Expert Line easy3D STED microscope system	Aberior	N/A
LSM 800 confocal laser scanning microscope system	Zeiss	N/A

Lattice Lightsheet 7 microscope system	Zeiss	N/A

Methods and Protocols

Cell lines and culture

Experiments were carried out using human hTERT-RPE1 (hTERT-immortalized retinal pigment epithelium) cells stably expressing CENP-A-GFP, human hTERT-RPE1 cells stably expressing both CENP-A-GFP and centrin1-GFP and human hTERT-RPE1 cells stably expressing CENP-A-GFP and Mis12-mCherry, all courtesy of Alexey Khodjakov (Wadsworth Center, New York State Department of Health, Albany, NY, USA), and human HeLa (cervical carcinoma patient) cells expressing GFP-Hec1-9A, courtesy of Geert Kops (Hubrecht Institute, Utrecht, The Netherlands). All cell lines were cultured in flasks in Dulbecco's Modified Eagle's Medium with 1 g/L D-glucose, pyruvate and L-glutamine (DMEM, Thermo Fisher, 11995065), supplemented with 10% (vol/vol) heat-inactivated Fetal Bovine Serum (FBS, Sigma-Aldrich, St. Louis, MO, USA) and penicillin (100 IU/mL)/streptomycin (100 mg/mL) solution (Lonza, Basel, Switzerland). The cells were kept at 37 °C and 5% CO2 in a humidified incubator (Galaxy 170 S CO2, Eppendorf, Hamburg, Germany) and regularly passaged at the confluence of 70-80%. None of the cell lines were authenticated. All cell lines have also been tested for mycoplasma contamination once a month by examining samples for extracellular DNA staining with SiR-DNA (100 nM, Spirochrome, Stein am Rhein, Switzerland) and Hoechst 33342 dye (1 drop/2 ml of NucBlue Live ReadyProbes Reagent, Thermo Fisher Scientific, Waltham, MA, USA) and have been confirmed to be mycoplasma free.

Sample preparation and siRNAs

At 80% confluence, the DMEM medium was removed from the flask and the cells were washed with 5 ml of phosphate buffered saline (PBS). Then, 1 ml 1% trypsin/ethylenediaminetetraacetic acid (EDTA, Biochrom AG, Berlin, Germany) was added to the flask and cells were incubated at 37 °C and 5% CO_2 in a humidified incubator for 5 min. After incubation, trypsin was blocked by adding 4 ml of DMEM medium. For the RNAi experiments, cells were seeded to reach 60% confluence the next day and cultured on 35 mm uncoated plates with 0.17 mm (#1.5 coverglass) glass thickness (MatTek Corporation, Ashland, MA, USA) in 1 ml of DMEM medium with the supplements described above. After one day of growth, cells were transfected with either targeting or non-targeting siRNA constructs which were diluted in OPTI-MEM medium (Thermo-Fisher) to a final concentration of 100 nM in the medium with cells. All transfections were performed 48 h before imaging using Lipofectamine RNAiMAX Reagent (Life Technologies, Waltham, MA, USA) according to the instructions provided by the manufacturer, unless otherwise indicated. Codepletions of Hec1 and CENP-E in HeLa cells were performed for two times in two subsequent days by the same protocol. After four hours of siRNA treatment, the medium was changed to the prewarmed DMEM medium. GFP-Hec1-9A construct in HeLa cells was expressed by addition of 1 $\mu g\ ml^{-1}$ doxycycline for 24 h prior to fixation. Proteasome inhibitor MG-132 (Merck, M7449,

IC50 value 100 nM) at a final concentration of 1 μM, was added 5 h before fixation for experiments involving HeLa GFP-Hec1-9A cells.

The siRNA constructs used were: human CENP-E ON-TARGETplus SMART pool siRNA (L-003252-00-0010, human custom-made 3'UTR HEC1 siRNA (oligo #3, Thermo Fisher Scientific; sequence 5′-CCCUGGGUCGUGUCAGGAA-3′), and control siRNA (D-001810-10-05, Dharmacon, Lafayette, CO, USA).

Drug treatments and drug washouts

CENP-E inhibitor GSK-923295 (MedChemExpress, Monmouth Junction, NJ, USA, IC50 value 3.2 nM) at a final concentration of 80 nM for RPE-1, was added 1-4 hours before imaging in most experiments, or when noted acutely before imaging. Eg5 inhibitor Monastrol (HY-101071A/CS-6183, MedChemExpress, IC_{50} value 50 μM) at a final concentration of 100 μM, was added 3 hours before imaging or acutely before imaging when noted. Aurora A inhibitor MLN8237 (MedChemExpress, IC_{50} value 4 nM) at a final final concentration of 125 nM or 250 nM as noted, was added acutely before imaging or 30-60 minutes before fixation. PLK4 inhibitor Centrinone (MedChemExpress, K_i value 0.16 nM) at a final concentration of 300 nM, was added 1-5 days before the imaging as noted.

The stock solutions for all drugs were prepared in DMSO. The stock solutions of all drugs were kept aliquoted at 10-50 μL at -20 °C for a maximum period of three months or at -80 °C for a maximum period of six months. New aliquots were thawed weekly for each new experiment. All drugs were added to DMEM media used for cell culture to obtain the final concentration of a drug as described. Drug washouts were performed by replacing drug-containing medium with 2 mL of fresh pre-warmed DMEM medium followed by four subsequent washouts with 2 mL of pre-warmed DMEM.

To deplete centrioles, Plk4 kinase activity was inhibited with centrinone, a small molecule inhibitor that blocks the centriole duplication cycle, and varied the duration of treatment to obtain spindles with different numbers of centrioles on each centrosome, a method established previously (Wong et al., 2015). Subsequently, we treated Plk4-inhibited cells with CENP-E inhibitor or DMSO and imaged cells a few hours after treatment using the same live cell imaging protocol described previously.

After acute treatment of CENP-E inhibited cells with the Eg5 inhibitor monastrol (50 uM), spindles quickly shortened, as expected from previous reports (Vukušić et al., 2021). Similarly, acute and drastic spindle shortening was observed in most CENP-E inhibited cells after acute addition of the Aurora A inhibitor MLN8237 (125 nM), as expected from previous studies (Ye et al., 2015).

Regarding cells imaged by confocal microscopy after the chronic inhibition of CENP-E by GSK-923295 (80 nM), all pseudo-metaphase spindles chosen for imaging were phenotypically similar between each other and between conditions where CENP-E was depleted or reactivated after washout of the CENP-E inhibitor: 1) in all cells few chromosomes were localized close to one of the spindle poles, called polar chromosomes, and their numbers ranged from 2-16 per cell; 2) occasionally in some cells few chromosomes were localized already in between spindle pole and

equator; and 3) in all cells most chromosomes were already aligned and tightly packed at the metaphase plate. This type of chromosome arrangement was expected from previously published data that reported that only 10-30% of chromosomes upon NEBD require CENP-E-mediated alignment (Barisic et al., 2014). Likewise, under all conditions where CENP-E was perturbed and cells imaged by confocal microscopy during pseudo-metaphase, the overall displacement of spindle poles from each other was negligible (data not shown), consistent with cells being in a pseudo-metaphase state where there is no net change in spindle length. For LLSM-based assay, no inclusion criteria for imaging were used as the cells were non-synchronized and entered mitosis stochastically. Only randomly selected cells that entered mitosis and subsequently entered anaphase during imaging time were used for kinetochore and centrosome tracking analysis.

Immunofluorescence

For cell labeling with phopho-Knl1, phopho-Dsn1, phosphor-Hec1, phospho-Aurora A, phospho-Aurora B, phospho-AuroraA/B/C, RPE-1 cells expressing CENP-A-GFP and centrin1-GFP grown on glass-bottom dishes (14 mm, No. 1.5, MatTek Corporation, Darmstadt, Germany) were pre-extracted with pre-warmed PEM buffer at 37 °C (0.1 M PIPES, 0.001 M MgCl2 × 6 H2O, 0.001 M EDTA, 0.5% Triton-X-100) for 30 s at room temperature and fixed by 1 ml of pre-warmed solution of 4% paraformaldehyde (PFA) for 20 min. All other antibodies were used on cells fixed for 2 minutes with ice-cold methanol, except for those used in STED microscopy, which are described below. After fixation, cells were washed 3 times for 5 min with 1 ml of PBS and permeabilized with 0.5% Triton-X-100 solution in water for 30 min at room temperature. To block unspecific binding, cells were incubated in 1 ml of blocking buffer (2% bovine serum albumin, BSA) for 2 h at room temperature. The cells were then washed 3 times for 5 min with 1 ml of PBS and incubated with 500 µl of primary antibody solution overnight at 4°C. Antibody incubation was performed using a blocking solution composed of 0.1% Triton, 1% BSA in PBS.

Following primary antibodies were used: rabbit monoclonal phopho-Knl1 (1.5 mg/ml, gift from J. Welburn, diluted 1:1000), rabbit monoclonal phopho-Dsn1 conjugated to Cy3 (0.5 mg/ml, gift from J. Welburn, diluted 1:250, diluted 1:500), rabbit monoclonal phospho-Aurora A (Thr288) (C39D8) (3079T, Cell Signaling Technology, diluted 1:500), rabbit monoclonal phospho-Aurora A (Thr288)/Aurora B (Thr232)/Aurora C (Thr198) (D12A11) (2914T, Cell Signalling Technology, diluted 1:500), rabbit polyclonal phospho-Hec1 (Ser55) (GTX70017, GeneTex, diluted 1:500), rabbit polyclonal phospho-Aurora B (Thr232) (GTX85607, GeneTex, diluted 1:500), rabbit monoclonal Anti-NDC80 (HPA066330-100uL, Sigma-Aldrich, diluted 1:250).

After primary antibody, cells were washed in PBS and then incubated in 500 µL of secondary antibody solution for 1 h at room temperature. Following secondary antibodies were used: Donkey anti-rabbit IgG Alexa Fluor 647 (ab150075, Abcam, diluted 1:1000) for phopho-Dsn1, Donkey anti-rabbit IgG Alexa Fluor 594 (ab150064, Abcam, diluted 1:1000) for all other rabbit antibodies, Donkey anti-mouse IgG Alexa Fluor 594 (ab150108, Abcam, diluted, 1:1000) for all mouse antibodies. Finally, cells were washed with 1 ml of PBS, 3 times for 10 min. Cells were imaged either immediately following the imaging or were kept at 4°C before imaging for a maximum period of one week.

To visualize alpha-tubulin in STED resolution in the RPE-1 CENP-A-GFP centrin1-GFP cell line, the ice-cold methanol protocol was avoided because it destroyed the unstable fraction of microtubules (Ponjavić et al., 2021). Cells were washed with cell extraction buffer (CEB) and fixed with 3.2% paraformaldehyde (PFA) and 0.1% glutaraldehyde (GA) in PEM buffer (0.1 M PIPES, 0.001 M MgCl2 × 6 H2O, 0.001 M EGTA, 0.5% Triton-X-100) for 10 min at room temperature. After fixation with PFA and GA, for quenching, cells were incubated in 1 ml of freshly prepared 0.1% borohydride in PBS for 7 min and then in 1 mL of 100 mM NH_4Cl and 100 mM glycine in PBS for 10 min at room temperature. To block nonspecific binding of antibodies, cells were incubated in 500 µL blocking/permeabilization buffer (2% normal goat serum and 0.5% Triton-X-100 in water) for 2 h at room temperature. Cells were then incubated in 500 µL of primary antibody solution containing rat anti-alpha-tubulin YL1/2 (MA1-80017, Invitrogen, CA, SAD, diluted 1:500) overnight at 4 °C. After incubation with a primary antibody, cells were washed 3 times for 10 min with 1 ml of PBS and then incubated with 500 µl of secondary antibody containing donkey anti-rat IgG Alexa Fluor 594 (ab150156, Abcam, diluted 1:300) for 2 h at room temperature, followed by wash with 1 ml of PBS 3 times for 10 min.

Imaging

The STED confocal microscope system (Abberior Instruments) and the LSM800 laser scanning confocal system (Zeiss) were used for the live-cell experiments we termed the confocal-based imaging assay. STED microscopy was also used to image all fixed cells in super-resolution. STED microscopy was performed using an Expert Line easy3D STED microscope system (Abberior Instruments, Göttingen, Germany) with the 100 x/1.4NA UPLSAPO100x oil objective (Olympus, Tokio, Japan) and an avalanche photodiode detector (APD). The 488 nm line was used for excitation, with the addition of the 561 nm line for excitation and the 775 nm laser line for depletion during STED super-resolution imaging. The images were acquired using Imspector software. The xy pixel size for fixed cells was 20 nm and 10 focal planes were acquired with a 300 nm distance between the planes. For confocal live cell imaging of cells, the xy pixel size was 80 nm and 16 focal images were acquired, with 0.5 µm distance between the planes and 1 min time intervals between different frames. During imaging, live cells were kept at 37 ° C and at 5% CO_2 in the Okolab stage incubation chamber system (Okolab, Pozzuoli, NA, Italy).

LSM 800 confocal laser scanning microscope system (Zeiss) was used for the rest of fixed-cell confocal-based imaging in hTERT-RPE1 cells expressing CENP-A-GFP and centrin1-GFP with the following parameters: sampling in xy, 0.27 µm; z step size, 0.5 µm; total number of slices, 32; pinhole, 48.9 µm; unidirectional scan speed, 10; averaging, 2; 63x Oil DIC f/ELYRA objective (1.4 NA), 488 nm laser line (0.1% power), and detection ranges of 410–558 nm. Images were acquired using ZEN 2.6 (blue edition; Zeiss). Imaging was done on multiples positions determined by the user and at the confocal lateral resolution.

The Lattice Lightsheet 7 microscope system (Zeiss) was used for live cell imaging of hTERT-RPE1 cells expressing CENP-A-GFP and Centrin1-GFP in assay we termed the LLSM-based imaging assay. The system was equipped with an illumination objective lens 13.3×/0.4 (at a 30° angle to cover the glass) with a static phase element and a detection objective lens 44.83×/1.0 (at a 60° angle to cover the glass) with an Alvarez manipulator. Images were acquired using ZEN 2.6

(blue edition; Zeiss). The automatic immersion of water was applied from the motorized dispenser at an interval of 20 or 30 minutes. Right after sample mounting, four steps of the 'create immersion' auto immersion option were applied. The sample was illuminated with a 488-nm diode laser (power output 10 Mw) with laser power set to 1-2%. The detection module consisted of a Hamamatsu ORCA-Fusion sCMOS camera with exposure time set to 15-20 ms. The LBF 405/488/561/642 emission filter was used. During imaging, cells were kept at 37 °C and at 5% CO2 in a Zeiss stage incubation chamber system (Zeiss). The width of the imaging area in the x dimension was set from 1 to 1.5 mm.

Tracking of centrosomes and kinetochores

The spatial x and y coordinates of the kinetochore pairs were extracted in each time frame using the Low Light Tracking Tool (v.0.10), an ImageJ plugin based on the Nested Maximum Likelihood Algorithm, as previously described (Vukušić et al., 2021). Tracking of polar kinetochores in the x and y planes was performed on the maximum intensity projections of all acquired z planes. Some kinetochore pairs could not be successfully tracked in all frames, mainly owing to cell and spindle movements in the z-direction over time. Spindle poles were manually tracked with points placed between the center of the two centrioles or centriole in centrinone treated cells. Kinetochore pairs that were aligned at the start of the imaging in a confocal-based imaging assay were also manually tracked in two dimensions. Quantitative analysis of all parameters was performed using custom-made MATLAB scripts (MatlabR2021a 9.10.0) scripts.

Due to the inability to reliably track polar kinetochores across all time frames due to neighboring kinetochores, tracking of polar kinetochores routinely commenced a few frames before the kinetochore pair began moving towards the equatorial plane. In the CENP-E reactivation assay, kinetochores were tracked from the onset of imaging until the successful identification of the same kinetochore pair, which occurred when the kinetochore pair was lost in the imaging plane, among other kinetochores, or when the imaging session ended, whichever came first. Aligned kinetochore pairs were tracked in the confocal-based assay using the same protocol.

Quantification of mean pHec1, pKnl1, pAurora A, pAuroraB intensities of kinetochore pairs

The fluorescence intensity signal of each kinetochore in both CENP-A and respective kinetochore protein channel (pDsn1, pKnl1) was measured by using the "*Oval selection*" tool in ImageJ with the size and position defined by the borders of the CENP-A signal of each kinetochore in the sum intensity projection of all acquired z-planes. pAurora A signal was measured using the "*Oval selection*" tool around the centriole signal as the center or around the signal of the Aurora A of the same size on the pole without centriole. The background fluorescence intensity measured in the cytoplasm was subtracted from the obtained values, and the calculated integrated intensity value was divided by the number of z-stacks used to generate the sum projection of each cell. The obtained mean intensity value subtracted for background for each kinetochore was normalized to the intensity of the CENP-A signal. For the pHec1 labeling experiments, the mean signal of Hec1 and CENP-A was measured by the same approach but on one z-plane where kinetochore CENP-A signal was the highest. The mean signal of the pAurora B was measured between extent of CENP-A signals of sister kinetochore pairs, and the mean value was normalized to mean value of

CENP-A signal of each sister kinetochore pair. All movies used for the analysis were performed using the same fixation protocol and were imaged with the same imaging parameters in at least three independent biological replicates. To avoid measurement of non-specific labeling of the spindle poles that are known artefacts of phospho-antibodies to kinetochore proteins (pAurB, pKnl1, pHec1) (Welburn et al., 2010), only the kinetochores outside of the circular pole signal (~1 μm from the centrosome) were measured and used for analysis.

Quantification of mean signal intensities of proteins after RNAi interreference

The fluorescence intensity signals were measured in triplicate samples for targeting and non-targeting groups for each siRNA treatment. Each siRNA targeting and non-targeting triplicates were imaged by the same protocol. All proteins were measured in mitotic cells at their respective locations during mitosis by using the "*Polygon selection tool*", as established by many previous studies: kinetochores and chromosomes defined by the DAPI or CENP-A area on sum of all acquired planes for Hec1 defined by the DAPI signal.

Quantification of polar kinetochore pairs

Polar kinetochores in all experiments were defined as kinetochore pairs that are closer to one of the spindle poles than to the equatorial plane. In confocal-based experiments polar chromosomes were defined from the onset of imaging. In cells treated with centrinone and their respective DMSO controls, the number of polar chromosomes was measured in time when the spindle finished the bipolarization process, e.g., the elongation of the spindle. This was done because all spindles of the 1:0 type with only one centriole at the beginning of mitosis went into the monopolar state and stayed in this state for variable durations before bipolarization, ranging from 10 to 50 minutes, as reported previously (Dudka et al., 2019). The residence time of polar chromosomes on spindle poles was defined as a time from spindle bipolarization until the last polar entered the metaphase plate, or a cell entered anaphase with uncongressed polar chromosome. Duration of mitosis was defined as the time from the first signs of nuclear envelope breakdown to one frame before visible onset of anaphase defined by the separation of sister kinetochore pairs.

Congression velocity was calculated for each pair of kinetochores in the last 6 minutes before the center of the pair of kinetochores surpassed 2 μm from the equatorial plane measured as the nearest distance from a center of a pair to a plane. These times represent the fast kinetochore movement towards the plate. Aligned kinetochore pair was defined as every pair that was found 3 μm from the equatorial plane at any given time. The equatorial or metaphase plane was defined in each time frame as the line perpendicular to the line connecting the centrosomes at their midpoint. The angle between the kinetochore pairs and the main spindle axis was defined as an angle between a line connecting two centrosomes and a line connecting the center of the kinetochore pair and a spindle pole nearest to the respective pair.

Image processing and statistical analysis

Image processing was performed in ImageJ (National Institutes of Health, Bethesda, MD, USA). Quantification and statistical analysis were performed in MatLab. The figures were assembled in Adobe Illustrator CS6 (Adobe Systems, Mountain View, CA, USA). Raw images were used for

quantification. The images of spindles were rotated in every frame to fit the long axis of the spindle to be parallel with the central long axis of the box in ImageJ and the spindle short axis to be parallel with the central short axis of the designated box in ImageJ. The designated box sizes were cut to the same dimensions for all panels in the figures where the same experimental setups were used across the treatments. When comparing different treatments in channels in which the same protein was labeled, the minimum and maximum intensity of that channel was set to the values in the control treatment. When indicated, the smoothing of the images was performed using the "Gaussian blur" function in ImageJ (s=0.5-1.0). Colour-coded maximum intensity projections of the z-stacks were done using the "*Temporal colour code*" tool in Fiji by applying “16-color” or “Spectrum” lookup-table (LUT) or other LUT as indicated. For the generation of univariate scatter plots, the open Matlab extension “UnivarScatter” was used.

Data are given as mean ± standard deviation (s.t.d.), unless otherwise stated. The mean line was plotted to encompass a minimum of 60% of the data points for each treatment. Other dispersion measures used are defined in their respective figure captions or in Figure 1 and Appendix Figure S1 if the same measures are used across all figures. The exact values of n are given in the respective figure captions, where n represents the number of cells or the number of tracked kinetochore pairs, as defined for each n in the figure captions or tables. The number of independent biological replicates is also given in the figure captions. An independent experiment for acute drug treatments was defined by the separate addition of a drug to a population of cells in a dish. The number of cells imaged simultaneously ranged from 1 to 7, depending on the specific microscopy system used. The p values when comparing multiple classes were obtained using the one-way ANOVA test followed by Tukey's Honest Significant Difference (HSD) test (significance level was 5%). $p < 0.05$ was considered statistically significant, very significant if $0.001 < p < 0.01$ and extremely significant if $p < 0.001$. Values of all significant differences are given with the degree of significance indicated ($*0.01 < p < 0.05$, $**0.001 < p < 0.01$, $***p < 0.001$, $**** < 0.0001$). For the linear regression correlation measure between two parameters, the nonparametric Spearman correlation coefficient, termed rs, was used where $p<0.001$, calculated using the 'corr' function in Matlab (Statistics Toolbox R14). No statistical methods were used to predetermine the sample size. The experiments were not randomized and, except where stated, the investigators were not blinded to allocation during experiments and outcome evaluation.

REFERENCES

Auckland, P., and A.D. McAinsh. 2015. Building an integrated model of chromosome congression. *J. Cell Sci.* 128:3363–3374. doi:10.1242/JCS.169367.

Bakhoum, S.F., G. Genovese, and D.A. Compton. 2009. Deviant kinetochore microtubule dynamics underlie chromosomal instability. *Curr. Biol.* 19:1937–1942. doi:10.1016/J.CUB.2009.09.055.

Barisic, M., P. Aguiar, S. Geley, and H. Maiato. 2014. Kinetochore motors drive congression of peripheral polar chromosomes by overcoming random arm-ejection forces. *Nat. Cell Biol.* 16:1249–1256. doi:10.1038/NCB3060.

Barisic, M., and H. Maiato. 2015. Dynein prevents erroneous kinetochore-microtubule attachments in mitosis. *Cell Cycle*. 14:3356. doi:10.1080/15384101.2015.1089369.

Barisic, M., and G. Rajendraprasad. 2021. Mitotic poleward flux: Finding balance between microtubule dynamics and sliding. *Bioessays*. 43. doi:10.1002/BIES.202100079.

Barisic, M., R. Silva E Sousa, S.K. Tripathy, M.M. Magiera, A. V. Zaytsev, A.L. Pereira, C. Janke, E.L. Grishchuk, and H. Maiato. 2015. Microtubule detyrosination guides chromosomes during mitosis. *Science (80-.).* 348:799–803. doi:10.1126/SCIENCE.AAA5175.

Bischoff, J.R., L. Anderson, Y. Zhu, K. Mossie, L. Ng, B. Souza, B. Schryver, P. Flanagan, F. Clairvoyant, C. Ginther, C.S.M. Chan, M. Novotny, D.J. Slamon, and G.D. Plowman. 1998. A homologue of Drosophila aurora kinase is oncogenic and amplified in human colorectal cancers. *EMBO J.* 17:3052–3065. doi:10.1093/EMBOJ/17.11.3052.

Bolhaqueiro, A.C.F., B. Ponsioen, B. Bakker, S.J. Klaasen, E. Kucukkose, R.H. van Jaarsveld, J. Vivié, I. Verlaan-Klink, N. Hami, D.C.J. Spierings, N. Sasaki, D. Dutta, S.F. Boj, R.G.J. Vries, P.M. Lansdorp, M. van de Wetering, A. van Oudenaarden, H. Clevers, O. Kranenburg, F. Foijer, H.J.G. Snippert, and G.J.P.L. Kops. 2019. Ongoing chromosomal instability and karyotype evolution in human colorectal cancer organoids. *Nat. Genet.* 51:824–834. doi:10.1038/S41588-019-0399-6.

Cai, S., C.B. O'Connell, A. Khodjakov, and C.E. Walczak. 2009. Chromosome congression in the absence of kinetochore fibres. *Nat. Cell Biol.* 11:832–838. doi:10.1038/NCB1890.

Cheerambathur, D.K., R. Gassmann, B. Cook, K. Oegema, and A. Desai. 2013. Crosstalk between microtubule attachment complexes ensures accurate chromosome segregation. *Science (80-.).* 342:1239–1242. doi:10.1126/SCIENCE.1246232/SUPPL_FILE/CHEERAMBATHUR.SM.PDF.

Cheeseman, I.M., J.S. Chappie, E.M. Wilson-Kubalek, and A. Desai. 2006. The Conserved KMN Network Constitutes the Core Microtubule-Binding Site of the Kinetochore. *Cell*. 127:983–997. doi:10.1016/J.CELL.2006.09.039.

Conduit, P.T., A. Wainman, and J.W. Raff. 2015. Centrosome function and assembly in animal cells. *Nat. Rev. Mol. Cell Biol.* 16:611–624. doi:10.1038/NRM4062.

Craske, B., and J.P.I. Welburn. 2020. Leaving no-one behind: how CENP-E facilitates

chromosome alignment. *Essays Biochem.* 64:313. doi:10.1042/EBC20190073.

DeLuca, J.G., W.E. Gall, C. Ciferri, D. Cimini, A. Musacchio, and E.D. Salmon. 2006. Kinetochore Microtubule Dynamics and Attachment Stability Are Regulated by Hec1. *Cell*. 127:969–982. doi:10.1016/J.CELL.2006.09.047.

DeLuca, K.F., S.M.A. Lens, and J.G. DeLuca. 2011. Temporal changes in Hec1 phosphorylation control kinetochore–microtubule attachment stability during mitosis. *J. Cell Sci.* 124:622–634. doi:10.1242/JCS.072629.

DeLuca, K.F., A. Meppelink, A.J. Broad, J.E. Mick, O.B. Peersen, S. Pektas, S.M.A. Lens, and J.G. DeLuca. 2018. Aurora A kinase phosphorylates Hec1 to regulate metaphase kinetochore-microtubule dynamics. *J. Cell Biol.* 217:163–177. doi:10.1083/jcb.201707160.

Dudka, D., C. Castrogiovanni, N. Liaudet, H. Vassal, and P. Meraldi. 2019. Spindle-Length-Dependent HURP Localization Allows Centrosomes to Control Kinetochore-Fiber Plus-End Dynamics. *Curr. Biol.* 29:3563-3578.e6. doi:10.1016/J.CUB.2019.08.061.

Eibes, S., G. Rajendraprasad, C. Guasch-Boldu, M. Kubat, Y. Steblyanko, and M. Barisic. 2023. CENP-E activation by Aurora A and B controls kinetochore fibrous corona disassembly. *Nat. Commun. 2023 141*. 14:1–14. doi:10.1038/s41467-023-41091-2.

Ertych, N., A. Stolz, A. Stenzinger, W. Weichert, S. Kaulfuß, P. Burfeind, A. Aigner, L. Wordeman, and H. Bastians. 2014. Increased microtubule assembly rates influence chromosomal instability in colorectal cancer cells. *Nat. Cell Biol.* 16:779–791. doi:10.1038/NCB2994.

Etemad, B., T.E.F. Kuijt, and G.J.P.L. Kops. 2015. Kinetochore–microtubule attachment is sufficient to satisfy the human spindle assembly checkpoint. *Nat. Commun. 2015 61*. 6:1–8. doi:10.1038/ncomms9987.

Famulski, J.K., and G.K. Chan. 2007. Aurora B kinase-dependent recruitment of hZW10 and hROD to tensionless kinetochores. *Curr. Biol.* 17:2143–2149. doi:10.1016/J.CUB.2007.11.037.

Ferreira, L.T., and H. Maiato. 2021. Prometaphase. *Semin. Cell Dev. Biol.* 117:52–61. doi:10.1016/j.semcdb.2021.06.004.

Ganem, N.J., S.A. Godinho, and D. Pellman. 2009. A mechanism linking extra centrosomes to chromosomal instability. *Nat. 2009 4607252*. 460:278–282. doi:10.1038/nature08136.

Görgün, G., E. Calabrese, T. Hideshima, J. Ecsedy, G. Perrone, M. Mani, H. Ikeda, G. Bianchi, Y. Hu, D. Cirstea, L. Santo, Y.T. Tai, S. Nahar, M. Zheng, M. Bandi, R.D. Carrasco, N. Raje, N. Munshi, P. Richardson, and K.C. Anderson. 2010. A novel Aurora-A kinase inhibitor MLN8237 induces cytotoxicity and cell-cycle arrest in multiple myeloma. *Blood*. 115:5202–5213. doi:10.1182/BLOOD-2009-12-259523.

Iemura, K., T. Natsume, K. Maehara, M.T. Kanemaki, and K. Tanaka. 2021. Chromosome oscillation promotes Aurora A-dependent Hec1 phosphorylation and mitotic fidelity. *J. Cell Biol.* 220. doi:10.1083/JCB.202006116.

Kapoor, T.M., M.A. Lampson, P. Hergert, L. Cameron, D. Cimini, E.D. Salmon, B.F. McEwen,

and A. Khodjakov. 2006. Chromosomes can congress to the metaphase plate before biorientation. *Science (80-.).* 311:388–391. doi:10.1126/SCIENCE.1122142.

Khodjakov, A., R.W. Cole, B.R. Oakley, and C.L. Rieder. 2000. Centrosome-independent mitotic spindle formation in vertebrates. *Curr. Biol.* 10:59–67. doi:10.1016/S0960-9822(99)00276-6.

Kim, Y., A.J. Holland, W. Lan, and D.W. Cleveland. 2010. Aurora kinases and protein phosphatase 1 mediate chromosome congression through regulation of CENP-E. *Cell*. 142:444–455. doi:10.1016/J.CELL.2010.06.039.

Klaasen, S.J., M.A. Truong, R.H. van Jaarsveld, I. Koprivec, V. Štimac, S.G. de Vries, P. Risteski, S. Kodba, K. Vukušić, K.L. de Luca, J.F. Marques, E.M. Gerrits, B. Bakker, F. Foijer, J. Kind, I.M. Tolić, S.M.A. Lens, and G.J.P.L. Kops. 2022. Nuclear chromosome locations dictate segregation error frequencies. *Nature*. 607:604–609. doi:10.1038/S41586-022-04938-0.

Kops, G.J.P.L., A.T. Saurin, and P. Meraldi. 2010. Finding the middle ground: How kinetochores power chromosome congression. *Cell. Mol. Life Sci.* 67:2145–2161. doi:10.1007/s00018-010-0321-y.

Leça, N., F. Barbosa, S. Rodriguez-Calado, M. Moura, P.D. Pedroso, I. Pinto, A.E. Verza, T. Bange, C.E. Sunkel, M. Barisic, T.J. Maresca, and C. Conde. 2024. Proximity-based activation of AURORA A by MPS1 potentiates error correction. *bioRxiv Prepr. Serv. Biol.* doi:10.1101/2024.06.11.598300.

Magidson, V., C.B. O'Connell, J. Lončarek, R. Paul, A. Mogilner, and A. Khodjakov. 2011. The spatial arrangement of chromosomes during prometaphase facilitates spindle assembly. *Cell*. 146:555–567. doi:10.1016/J.CELL.2011.07.012.

Maiato, H., A.M. Gomes, F. Sousa, and M. Barisic. 2017. Mechanisms of Chromosome Congression during Mitosis. *Biol. 2017, Vol. 6, Page 13*. 6:13. doi:10.3390/BIOLOGY6010013.

Manandhar, G., H. Schatten, and P. Sutovsky. 2005. Centrosome Reduction During Gametogenesis and Its Significance. *Biol. Reprod.* 72:2–13. doi:10.1095/BIOLREPROD.104.031245.

McEwen, B.F., G.K.T. Chan, B. Zubrowski, M.S. Savoian, M.T. Sauer, and T.J. Yen. 2001. CENP-E is essential for reliable bioriented spindle attachment, but chromosome alignment can be achieved via redundant mechanisms in mammalian cells. *Mol. Biol. Cell*. 12:2776–2789. doi:10.1091/MBC.12.9.2776.

Navarro, A.P., and I.M. Cheeseman. 2021. Kinetochore assembly throughout the cell cycle. *Semin. Cell Dev. Biol.* 117:62–74. doi:10.1016/J.SEMCDB.2021.03.008.

Orr, B., F. De Sousa, A.M. Gomes, O. Afonso, L.T. Ferreira, A.C. Figueiredo, and H. Maiato. 2021. An anaphase surveillance mechanism prevents micronuclei formation from frequent chromosome segregation errors. *Cell Rep.* 37. doi:10.1016/J.CELREP.2021.109783.

Ponjavić, I., K. Vukušić, and I.M. Tolić. 2021. Expansion microscopy of the mitotic spindle. *Methods Cell Biol.* 161:247–274. doi:10.1016/BS.MCB.2020.04.014.

Renda, F., and A. Khodjakov. 2021. Role of spatial patterns and kinetochore architecture in spindle morphogenesis. *Semin. Cell Dev. Biol.* 117:75–85. doi:10.1016/j.semcdb.2021.03.016.

Renda, F., C. Miles, I. Tikhonenko, R. Fisher, L. Carlini, T.M. Kapoor, A. Mogilner, and A. Khodjakov. 2022. Non-centrosomal microtubules at kinetochores promote rapid chromosome biorientation during mitosis in human cells. *Curr. Biol.* doi:10.1016/J.CUB.2022.01.013.

Shrestha, R.L., D. Conti, N. Tamura, D. Braun, R.A. Ramalingam, K. Cieslinski, J. Ries, and V.M. Draviam. 2017. Aurora-B kinase pathway controls the lateral to end-on conversion of kinetochore-microtubule attachments in human cells. *Nat. Commun.* 8. doi:10.1038/S41467-017-00209-Z.

Sikirzhytski, V., F. Renda, I. Tikhonenko, V. Magidson, B.F. McEwen, and A. Khodjakov. 2018. Microtubules assemble near most kinetochores during early prometaphase in human cells. *J. Cell Biol.* 217:2647–2659. doi:10.1083/JCB.201710094.

Stolz, A., N. Ertych, A. Kienitz, C. Vogel, V. Schneider, B. Fritz, R. Jacob, G. Dittmar, W. Weichert, I. Petersen, and H. Bastians. 2010. The CHK2-BRCA1 tumour suppressor pathway ensures chromosomal stability in human somatic cells. *Nat. Cell Biol.* 12:492–499. doi:10.1038/NCB2051.

Tamura, N., N. Shaikh, D. Muliaditan, T.N. Soliman, J.R. McGuinness, E. Maniati, D. Moralli, M.-A. Durin, C.M. Green, F.R. Balkwill, J. Wang, K. Curtius, and S.E. McClelland. 2020. Specific Mechanisms of Chromosomal Instability Indicate Therapeutic Sensitivities in High-Grade Serous Ovarian Carcinoma. *Cancer Res.* 80:4946–4959. doi:10.1158/0008-5472.CAN-19-0852.

Tovini, L., and S.E. McClelland. 2019. Impaired CENP-E Function Renders Large Chromosomes More Vulnerable to Congression Failure. *Biomol. 2019, Vol. 9, Page 44*. 9:44. doi:10.3390/BIOM9020044.

Vasquez-Limeta, A., and J. Loncarek. 2021. Human centrosome organization and function in interphase and mitosis. *Semin. Cell Dev. Biol.* 117:30–41. doi:10.1016/j.semcdb.2021.03.020.

Vukušić, K., I. Ponjavić, R. Buđa, P. Risteski, and I.M. Tolić. 2021. Microtubule-sliding modules based on kinesins EG5 and PRC1-dependent KIF4A drive human spindle elongation. *Dev. Cell*. 56:1253-1267.e10. doi:10.1016/J.DEVCEL.2021.04.005/ATTACHMENT/680C448C-DA20-433C-9F27-C90D96D86C9D/MMC1.PDF.

Vukušić, K., and I.M. Tolić. 2024. CENP-E initiates chromosome congression by opposing Aurora kinases to promote end-on attachments. *bioRxiv*, doi:10.1101/2023.10.19.563150.

Welburn, J.P.I., M. Vleugel, D. Liu, J.R. Yates, M.A. Lampson, T. Fukagawa, and I.M. Cheeseman. 2010. Aurora B Phosphorylates Spatially Distinct Targets to Differentially Regulate the Kinetochore-Microtubule Interface. *Mol. Cell*. 38:383–392. doi:10.1016/J.MOLCEL.2010.02.034.

Willems, E., M. Dedobbeleer, M. Digregorio, A. Lombard, P.N. Lumapat, and B. Rogister. 2018. The functional diversity of Aurora kinases: a comprehensive review. *Cell Div.* 13. doi:10.1186/S13008-018-0040-6.

Wong, Y.L., J. V. Anzola, R.L. Davis, M. Yoon, A. Motamedi, A. Kroll, C.P. Seo, J.E. Hsia, S.K. Kim, J.W. Mitchell, B.J. Mitchell, A. Desai, T.C. Gahman, A.K. Shiau, and K. Oegema. 2015. Reversible centriole depletion with an inhibitor of Polo-like kinase 4. *Science*. 348:1155. doi:10.1126/SCIENCE.AAA5111.

Ye, A.A., J. Deretic, C.M. Hoel, A.W. Hinman, D. Cimini, J.P. Welburn, and T.J. Maresca. 2015. Aurora A Kinase Contributes to a Pole-Based Error Correction Pathway. *Curr. Biol.* 25:1842–1851. doi:10.1016/J.CUB.2015.06.021.

SUPPLEMENTARY FIGURE LEGENDS

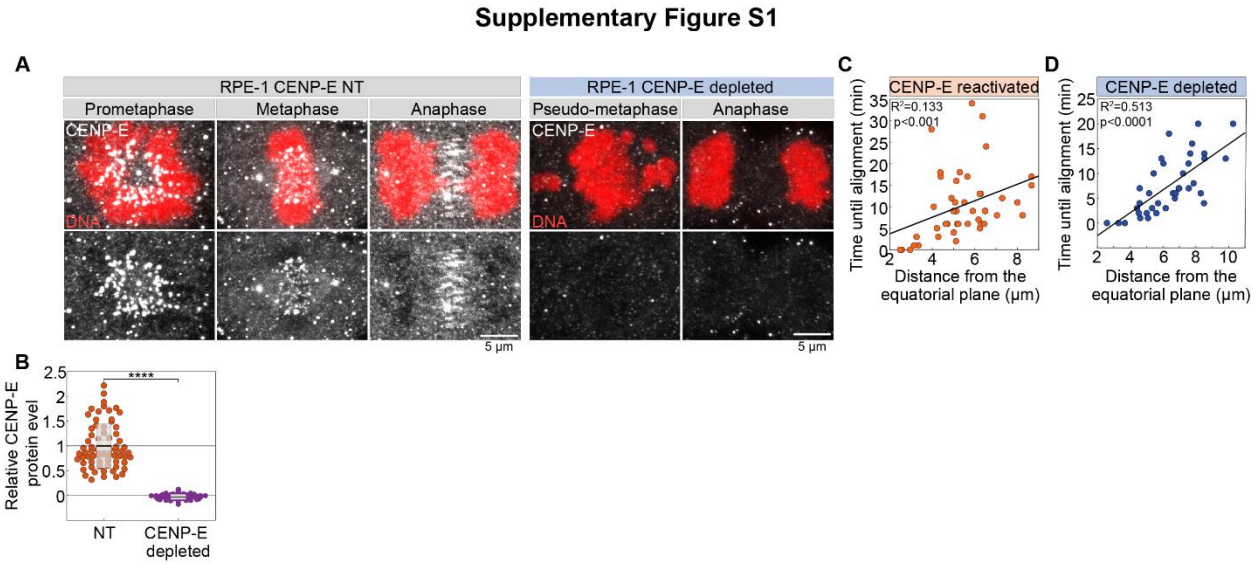

Figure S1. Speed of congression initiation is correlated with the distance of polar chromosome from the centrosome, related to Figure 1. (A) Representative examples of RPE-1 cells after treatment with non-targeting (NT) small interfering RNAs (siRNAs) (left) or CENP-E siRNA (right) and immunofluorescence with antibodies targeting CENP-E, in different stages of mitosis as labeled. RPE-1 cells were wild-type (WT) and stained with DAPI (red). Top images represent maximum projections with merged channels, and bottom images represent only the channel in gray, representing the signal of the antibody targeting CENP-E. (B) Average CENP-E protein level relative to the average of the non-targeting control group for depicted proteins. Numbers: 62, 57 cells. (C and D) Distance to the equatorial plane of the polar kinetochore pairs versus the time of alignment of each pair in the cells after washing out the CENP-E inhibitor (C) and the depletion of CENP-E (D), where the line represents regression. Statistics: Tukey's HSD test. Symbols indicate: n.s. $P > 0.05$, **$P \leq 0.01$, ***$P \leq 0.001$, ****$P \leq 0.0001$.

Supplementary Figure S2

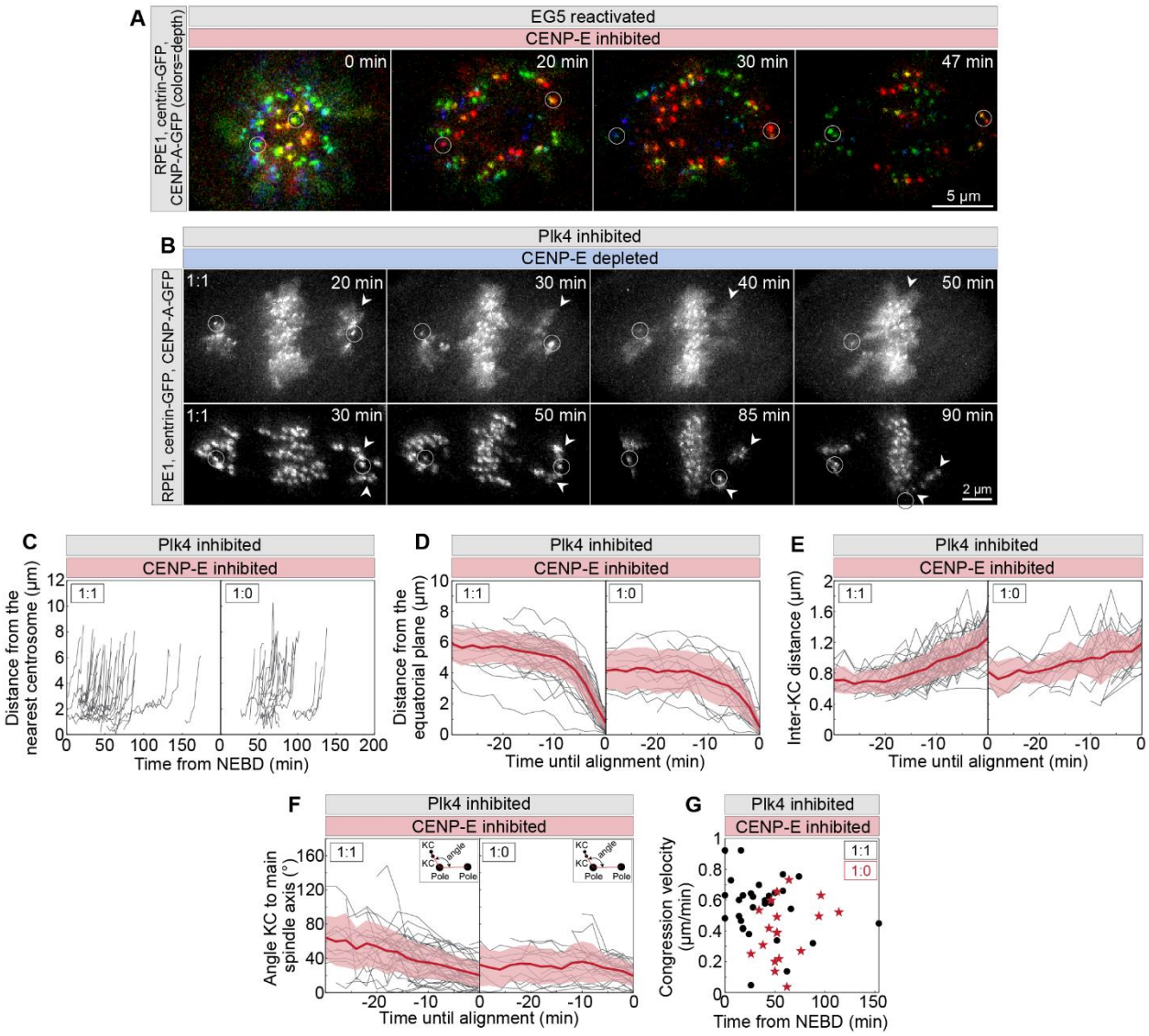

Figure S2. Chromosome movement during congression is similar in cells with different numbers of centrioles, related to Figure 1. (A) Representative example of an RPE1 cell expressing CENP-A-GFP and centrin1-GFP (circled) in different frames from the washout of the Eg5 inhibitor monastrol and acute inhibition of CENP-E by 80 nM GSK923295. Time 0 represents the time of the washout of monastrol and the addition of GSK923295. (B) Representative examples of RPE1 cells expressing CENP-A-GFP and centrin1-GFP in different frames from the onset of NEBD after depletion of CENP-E. Centrioles are rounded by the white circle. Arrowheads depict polar chromosomes that align after centriole separation from the centrosome. (C-F) Distance from the nearest spindle pole over time from nuclear envelope breakdown (NEBD) of initially polar kinetochore pairs (C), distance to the equatorial plane (D), interkinetochore (inter-KC) distance (E), and angle to the main spindle axis of kinetochore pairs, depicted in the scheme in the graph (F) over time until alignment for initially polar kinetochores in the presence of the CENP-E inhibitor for cells with different numbers of centrioles as indicated in the top left part of each graph.

Thick lines represent means, and pale areas around the means represent standard deviations. (G) Velocity of chromosome congression during the 6-minute period that precedes complete alignment for depicted treatment over time from the onset of mitosis for cells with the number of centrioles as indicated. KC, kinetochore.

Supplementary Figure 3

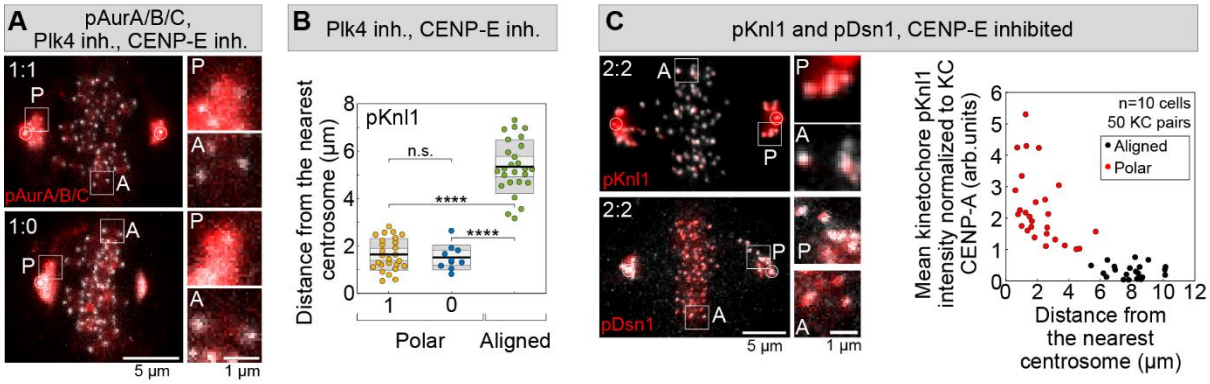

Figure S3. Aurora B-mediated phosphorylation declines gradually on outer-kinetochore substrates during congression of polar chromosomes, related to Figures 2 and 3. (A) Representative examples (left) and blowups of boxed regions from the left (right) of RPE-1 cells expressing CENP-A-GFP and centrin1-GFP (circled) immunostained with antibodies targeting pT288-Aurora A, pT232-Aurora B and pT198-Aurora C, with different numbers of centrioles on each spindle pole after 300 nM centrinone treatment and after acute treatment with DMSO (control) as indicated on the top. The images are maximum projections. A, aligned, P, polar. (B) Distance from a spindle pole of different groups of kinetochores as indicated at the bottom from the pKnl1 immunolabelling experiment after acute CENP-E inhibition. (C) Representative examples on the left and blowups of boxed regions on the right of RPE-1 cells expressing CENP-A-GFP and centrin1-GFP immunostained with antibodies targeting phosphorylated residues of pKnl1 (top left) and pDsn1 (pS100, pS109-Dsn1, bottom left) after inhibition of CENP-E activity (left) and plot of mean signal intensity of pKnl1 on polar and aligned kinetochore pairs versus the distance of pairs from the spindle pole (right). n.s., nonsignificant. Numbers: numbers for G are given in the legend of Figure 3. Statistics: Tukey's HSD test. Symbols indicate: n.s. $P > 0.05$, ****$P \leq 0.0001$. Inh., inhibited; KC, kinetochore.

VIDEO LEGENDS

Video 1. RPE1 cells stably expressing CENP-A-GFP and Centrin1-GFP in Plk4-inhibited cells with different number of centrioles in CENP-E inhibited and CENP-E depleted conditions imaged by confocal microscopy. RPE-1 cells stably expressing CENP-A-GFP and Centrin1-GFP (16-colors LUT) in cells treated with Plk4 inhibitor for 2 days with distinct number of centrioles on each centrosome (1:1, 1:0, and 0:0) and subsequently treated with CENP-E inhibitor for 3hr before imaging (CENP-E inhibited, left) and with CENP-E siRNA for 48hr before imaging (CENP-E depleted, right). Cells were imaged 48h after addition of CENP-E siRNA (left) or 3h after the addition of the drug (right). Kinetochores are color-coded for depth from blue to red with the 16 Colors LUT.